Single Image Defogging Based on Multi-Channel Convolutional MSRCR

WEIDONG ZHANG[ID][1]**, (Student Member, IEEE), LILI DONG**[1]**, XIPENG PAN**[2]**,
JINGCHUN ZHOU**[1]**, LI QIN**[3]**, AND WENHAI XU**[1]

[1]School of Information Science and Technology, Dalian Maritime University, Dalian 116026, China
[2]School of Automation, Beijing University of Posts & Telecommunications, Beijing 100876, China
[3]School of Information Science and Engineering, Ningbo University, Ningbo 315211, China

Corresponding author: Lili Dong (dll_lili@163.com)

ABSTRACT In order to solve the problem of image degradation in foggy weather, a single image defogging method based on a multi-scale retinex with color restoration (MSRCR) of multi-channel convolution (MC) is proposed. The whole defogging process mainly consists of four key parts: estimation of illumination components, guided filter operation, reconstruction of fog-free images, and white balance operation. First, the multi-scale Gaussian kernels are employed to extract precise features to estimate the illumination component. After that, the MSRCR method is applied to enhance the global contrast, detail information, and color restoration of the image. Second, the smoothing constraints of both illumination component and reflected component are considered together by using the guided filter twice, thus the enhanced image satisfies the smoothing constraint and the noise in the enhanced image is reduced. Third, the enhanced image by the MSRCR and the image processed by the secondary guided filter are fused by linear weighting to reconstruct the final fog-free image. Finally, in order to eliminate the influence of illumination on the color of the defogged image, the final defogged image is processed by white balance. The experimental results demonstrated that the proposed method can outperform state-of-the-art methods in both qualitative and quantitative comparisons.

INDEX TERMS Image defogging, multi-channel convolution, guided filter, weighted fusion, MSRCR.

I. INTRODUCTION

A clear image is a key prerequisite for understanding real-world scenarios in the field of digital imaging. In the outdoor environment, visibility and contrast of a photograph will seriously reduce due to bad weather such as light, fog and haze [1]–[3]. The main reason is that the quality of the photo is highly susceptible to scattering, refraction, and reflection of a large amount of small particles in the air before the light reaches the camera lens. In order to effectively remove dense fog and highlight the details of the image, image restoration and enhancement are commonly used methods [4]–[6]. Fig. 1 shows examples of dense fog images and their corresponding defogged images. As shown in the top row of Fig. 1, low-quality images greatly affect the perceptions and recognition capabilities of the human eyes. It can

be seen from the bottom row of Fig. 1 that the defogged images have better visual effects and clearer details, which are more suitable for applications in expanding areas such as space, transportation, meteorology, underwater detection, and military technology. Therefore, image defogging has become an important research direction, which has attracted more and more attention of researchers [1]–[6].

In recent decades, image defogging based on image enhancement and physical model has achieved good development [7]. The defogging method based on physical model could obtain the optimal estimation of fog-free images is obtained by establishing an approximate atmospheric scattering model and inversion degradation process [8]. It can be divided into three categories. The first category means using depth information [9], [10]. For example, Tarel *et al.* [9] and Kopf *et al.* [10] obtained the depth information of the image, and then solved the image degradation model to estimate the fog-free image. However, this kind of

FIGURE 1. Examples of dense fog and defogged images. The top row shows two fog images, the defogged images by our method on the bottom row.

method is highly targeted with high hardware requirements that limit its application in many fields. The second category means using atmospheric light polarization [11], [12]. Schechner and Averbuch [11] and Shwartz *et al.* [12] captured images under different brightness through polarizer to estimate polarization, ambient light intensity, and transmittance distribution to achieved rapid defogging. However, this kind of method has poor defogging effect in dense fog and cannot process a single image automatically. The third category means using prior information [13]–[15], He *et al.* [13], Nishino *et al.* [14] and Chen *et al.* [15] proposed to restore foggy images to fog-free images by acquiring prior information. However, this kind of method is difficult to acquire prior information and the time complexity is high. In short, the defogging method based on physical model needs some prior information of one or more images in the same scene, or requires some physical equipment, which is inconvenient in practical application [16].

The defogging method based on image enhancement can be detached from the dependence on physical devices and become the main research direction of current defogging method, which includes histogram equalization [17], homomorphic filter [18], bilateral filter [19], guided filter [20], and retinex method [21]–[23]. Histogram equalization [17] may enhance the contrast of background noise and reduce the contrast of usable signals because of it does not select the processed data. The computational complexity of homomorphic filtering and bilateral filtering is high, and the efficiency and practicability of the method are not satisfactory. As a local linear image filter, guided filter [20] has good edge preservation and smooth filtering performance. However, when the original image is complex and noisy, the enhanced image may appear noise enhancement. Image defogging methods based on Retinex theory include Single-scale

Retinex (SSR) [21], Multi-scale Retinex (MSR) [22], Multi-scale Retinex with color restoration (MSRCR) [23], and other improved methods. In these defogging methods, the estimation and elimination of illumination components are the key steps, and Gaussian filtering is usually used to estimate the illumination component. SSR [21] method was mainly used to enhance grayscale images, but it was difficult to balance the dynamic range compression and color constancy of the image. The MSR [22] method is a linear weighted fusion of multiple SSRs with different scales, which could enhance the color image, but would produce the problem of color degradation. MSRCR [23] introduced the color recovery factor on the basis of MSR, so that the enhanced image had better color guarantee, but the color of the image would deviate from the original color and the whole image tended to white. Tare *et al.* [24] used MSR method to remove fog in dense fog scenario for many objects. However, the defogging image is far from the fog-free image when the fog in the scenario was non-uniform, which indicated that MSR increased some contrasts corresponding to fog and not to the scene. Zhang *et al.* [25] employed the retinex to obtain the illumination component and used gamma correction to balance the image brightness. However, since the attenuation of illumination light was not considered, the image after defogging appeared local distortion and blurred details. Wang *et al.* [26] proposed an efficient single image defogging method based on physical model and MSRCR, which could be fast and efficient, but the defogged image appeared over-exposed and halo effect. Because of the good learning and representation ability of deep network structure, the single image defogging technology based on deep learning [27]–[29] has been widely promoted and applied.

In summary, defogging method based on image enhancement can be detached from the dependence on physical devices and has good application value. In order to take full advantage of the enhancements with the retinex and solve the problem of missing image detail information, a defogging model based on multi-channel convolutional MSRCR (MC_MSRCR) is proposed, which is combined by guided filtering and MSRCR, as well as introduces multi-channel convolution and linear weighted fusion. The main contributions of this paper include four aspects:

1) For the enhanced image of MSRCR, the smoothing constraints of both illumination component and reflected component are considered together by using guided filter twice, thus the enhanced image satisfies the smoothing constraint and the noise in the enhanced image is reduced.

2) In order to extract more precise features to estimate the illumination component, six Gaussian convolution kernels of different scales are used for multi-channel convolution. Meanwhile, the Retinex operation is carried out, and the quantization operation is introduced to ensure that the defogging image has good color fidelity.

3) The final defogging image is a linear weighted fusion of the image after secondary guided filtering processing and the MSRCR-based enhanced.
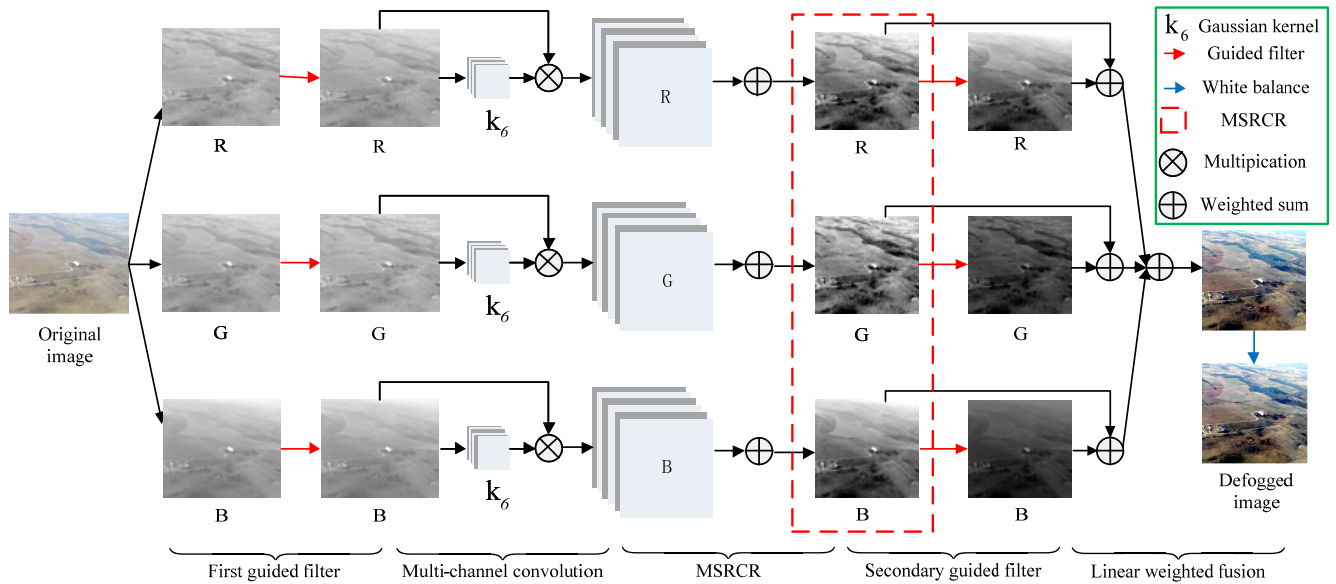
FIGURE 2. The framework of the proposed algorithm.

4) The final defogged image is processed by white balance to improve the visual effect of defogged image.

The rest of the paper is organized as follows. The proposed defogging method and its detail operation are shown in section II. Along with experimental results and analysis in section III, the performance of the proposed method in different applications is evaluated. The conclusion and the exploration of the future work are shown in section IV.

II. PROPOSED DEFOGGING MODEL

In this section, we will describe in detail the proposed defogging model in detail, as shown in Fig. 2. In the following, we describe the process and analyze the meaning of each step in detail. Firstly, the guided filtering processing of the original image preserves the edge information and overcomes the noise. Secondly, in order to extract more precise features to estimate the illumination component, the R, G and B channels after the guided filtering are convolution by six Gaussian convolution kernels of different scales, respectively, and then the corresponding six feature maps of the same size are obtained. Thirdly, the six feature maps corresponding to each channel are enhanced by MSRCR and merged with the linear weighting to improve the enhanced quality, and the quantization operation is introduced to ensure that the defogging image with good color fidelity. Meanwhile, the overflow judgment is introduced to ensure that the pixel-value of the defogged image is between $0 \sim 255$. Fourthly, since the first guided filter only considers the smoothing constraints on the illumination component, the final defogged image not only preserves the noise of the original image, but also enhances the estimation error of the illumination component. However, the smoothing constraints of both illumination component and reflected image are considered by using twice guided filter, so that the enhanced image satisfies the smoothing constraint and the noise in the enhanced image is reduced. Fifthly, the image enhanced by MSRCR and the image processed by secondary guided filter are fused with linear weighting to reconstruct the final fog-free image. Finally, in order to enhance the appearance of the defogged image by white balance processing.

A. FIRST GUIDED FILTER

The guided filter is a novel edge-preserving filter with edge smoothing and detail enhancement. Its output is a local linear transformation of the guided image. He *et al.* [20] gave the definition and introduced the detailed solution process of the guided filter, which is expressed as $q =$ guided_filter(p, I, r, ε) where p is the input image of the filter, I is the guiding image, r is the window size of the filter $\varepsilon > 0$ is the regularization coefficient, and q is the filtered image. As can be observed in Fig. 2, the original image is divided into R, G, and B channels. The guided filtering processing of R, G, and B channels are expressed as follows:

$$R_{GF}^1 = \text{guided\_filter}(R, R, r, \varepsilon) \quad (1)$$

$$G_{GF}^1 = \text{guided\_filter}(G, G, r, \varepsilon) \quad (2)$$

$$B_{GF}^1 = \text{guided\_filter}(B, B, r, \varepsilon) \quad (3)$$

where $r = 32$ and $\varepsilon = 0.01$, and they are determined by a large number of experiments.

B. MULTI-CHANNEL CONVOLUTION

Different convolution kernels can obtain different Feature maps of input image in CNN [27]–[29], and these Features maps are a representation of feature information. However, the complexity of the algorithm increases as the number of

convolution kernel increases. Therefore, it is necessary to determine the number of convolution kernel by weighing the amount of feature information and the time complexity of the algorithm. The estimation of illumination components in Retinex is convolution operation on the input image by Gaussian kernels of different scales. These images obtained by convolution of the input image by Gaussian kernels of different scales are like Feature maps in CNN. However, the traditional MSRCR method uses Gaussian kernel functions with three different scales to convolution R, G and B channels. Based on this consideration, the idea of multiple kernel convolutions is introduced into MSRCR method by referring to the ability of multiple kernel convolutions to extract precise features in CNN [27]–[29]. Firstly, six Gaussian convolution kernels of different scales were used for convolution of R, G, and B channels in order to extract precise features to estimate illumination components. Then, in order to enhance the detail information and global contrast of the image by a multi-scale linear weighted retinex operation is performed on the illumination component. The framework of multi-channel multi-scale convolution is shown in the second phase of Fig. 2, the estimation formula of the illumination component is expressed as follows:

$$L_i^n (Gf_i(x, y)) = S(Gf_i(x, y)) * G_n(x, y) \quad (4)$$

where $G(x, y) = \frac{1}{2\pi\sigma^2} \exp(-\frac{x^2+y^2}{2\sigma^2})$ is a Gaussian kernel function, n is the number of filter radius scales of the Gaussian filter and $\iint G(x, y)dxdy = 1$, we use six scales in actual applications ($n = 6$). Typically, two small scales are $0 \leq \sigma_1 \leq \sigma_2 < 50$, two medium scales are $50 \leq \sigma_3 \leq \sigma_4 < 100$, and two large scales are $100 \leq \sigma_5 < \sigma_6$. $Gf_i(x, y)$ is a guiding filter function of the original image. $L_i^n (Gf_i(x, y))$ is the illumination component corresponding to the nth scale of the ith channel.

C. MSRCR

The basic idea of retinex [21] is that the intensity of the reflected light is not a decisive factor in the color of an object, whereas it is determined by the ability of an object to reflect the light of a long, medium and short wave. That is, the reflection property of the object is preserved, and the influence of the illumination light on the original image is removed. According to retinex theory, an idea image is defined as follows:

$$S(x, y) = L(x, y) * R(x, y) \quad (5)$$

where $S(x, y)$ is an image observed in the real word or generated by other imaging devices, and $L(x, y)$ is an illumination component and $R(x, y)$ is a reflected image. Then, taking logarithm of both sides of equation (5)

$$\log(S(x, y)) = \log(L(x, y)) + \log(R(x, y)) \quad (6)$$

$R(x, y)$ can be expressed as follows:

$$\log(R(x, y)) = \log(S(x, y)) - \log(L(x, y)) \quad (7)$$

the detailed solution process of $L(x, y)$ is shown in section B, $L(x, y) = S(x, y) * G(x, y)$ and $G(x, y) = \frac{1}{2\pi\sigma^2} \exp(-\frac{x^2+y^2}{2\sigma^2})$ when $n = 1$. From (5), (6), and (7), we redefine $\log(R_i(x, y))$ as follows:

$$\log(R_i(x, y)) = \log(S_i(x, y)) - \log(S_i(x, y) * G(x, y)) \quad (8)$$

where i is a channel of the image. Equation (8) is actually a SSR algorithm, in order to compensate for shortcomings of the SSR, the MSR [22] improves the color image by linear weighting fusion of multiple SSRs with different scales, which is expressed as follows:

$$R_{MSR_i}(x, y) = \sum_{n=1}^{N} w_n \big[\log(S_i(x, y)) - \log(S_i(x, y) * G_n(x, y))\big] \quad (9)$$

where N is the number of scales $R_{MSR_i}(x, y)$ is the result of MSR processing on the ith channel, $G_n(x, y)$ is the Gaussian kernel function corresponding to the nth scale, and w_n is the weight corresponding to the nth scale.

Based on the research of image enhancement code in GIMP, mean and variance are introduced in the process of adjusting color deviation by directly starting from the quantitative operation. Meanwhile, a parameter D that controls the dynamic of the image is introduced to achieve the adjustment of colorless deviation, which significantly improves the color fidelity and better adaptation to a variety of images. Then the improved MSRCR [23] is defined as follows:

$$Min = Mean(R_{MSR_i}) - D \cdot Var(R_{MSR_i}) \quad (10)$$

$$Max = Mean(R_{MSR_i}) + D \cdot Var(R_{MSR_i}) \quad (11)$$

$$R_{MSRCR_i} = 255 * \frac{R_{MSR_i} - Mean(R_{MSR_i}) + D * Var(R_{MSR_i})}{2*D*Var(R_{MSR_i})} \quad (12)$$

where Mean and Var are the functions of mean and variance, respectively. In the GIMP source code, the researchers point out that enhanced images have a better dynamic compression range D with is 2~3. We verify through experiments that when D is set to 2 MSRCR enhanced images can better retain detail and restore the color of the image. For equation (12), an overflow judgment is added to ensure that all pixel values are between [0, 255], that is:

$$R_{MSRCR_i}(x, y) = \begin{cases} 255 & R_{MSRCR_i}(x, y) > 255 \\ 0 & R_{MSRCR_i}(x, y) < 0 \\ R_{MSRCR_i}(x, y) 0 \leq & R_{MSRCR_i}(x, y) \leq 255 \end{cases} \quad (13)$$

D. SECONDARY GUIDED FILTER

The first guided filtering only takes into account the smooth constraint on the illumination component. The result of the final defogged image preserves the noise of the original image and enhances the estimation error of the illumination component. However, the secondary guided filtering takes

into account both the smoothing constraints of the illumination component and the reflected image together, so that the image after secondary guided filtering processing satisfies the smoothing constraint condition and the noise in the enhanced image is reduced. The secondary guided filter of R_{MSRCR}, G_{MSRCR} and B_{MSRCR} channels is expressed as follows:

$$R_{GF}^2 = \text{guided\_filter}(R_{MSRCR}, R_{MSRCR}, r, \varepsilon) \quad (14)$$

$$G_{GF}^2 = \text{guided\_filter}(G_{MSRCR}, G_{MSRCR}, r, \varepsilon) \quad (15)$$

$$B_{GF}^2 = \text{guided\_filter}(B_{MSRCR}, B_{MSRCR}, r, \varepsilon) \quad (16)$$

where $r = 32$ and $\varepsilon = 0.01$, and they are determined by a large number of experiments.

E. LINEAR WEIGHTED FUSION
The detailed fusion steps are as follows.

Step 1: According to subsection *C*, we can know that R_{MSRCR}, G_{MSRCR}, and B_{MSRCR} are enhanced images by multichannel convolutional MSRCR.

Step 2: According to subsection *D*, we can know that R_{GF}^2, G_{GF}^2, and B_{GF}^2 are detailed images by secondary guided filter.

Step 3: Enhanced images and detailed images are obtained according to Step 1 and Step 2 respectively, then R, G and B channels are fused. From the linear weighted fusion formula [30], [31], it can be concluded that:

$$R(i,j) = \lambda R_{MSRCR}(i,j) + (1 - \lambda)R_{GF}^2(i,j) \quad (17)$$

$$G(i,j) = \lambda G_{MSRCR}(i,j) + (1 - \lambda)G_{GF}^2(i,j) \quad (18)$$

$$B(i,j) = \lambda B_{MSRCR}(i,j) + (1 - \lambda)B_{GF}^2(i,j) \quad (19)$$

it can be seen from Step 3 that the R, G, and B channels are fused by linear weighted fusion rules, and the fused R, G and B are synthesized into the final defogging image. We define the final fusion image can be expressed as follows. where λ is the weighted coefficient and $0 \le \lambda \le 1$. In this paper, the fusion image has a better visual effect λ with is 0.9~0.96, and the final λ is set to 0.95.

$$
\begin{aligned}
RGB\,(i,j) \\
&= R\,(i,j) + G\,(i,j) + B\,(i,j) \\
&= \sum_{I \in \{R,G,B\}} \left(I_{R_{GF}^2}(i,j) + \lambda \left(I_{MSRCR}(i,j) - I_{R_{GF}^2}(i,j) \right) \right)
\end{aligned}
$$
$$(20)$$

F. WHITE BALANCE
In order to eliminate the influence of illumination on the color of the defogged image, it will obtain the color characteristics of the surface of the object independent of the illumination. Finlayson and Trezzi [32] proposed a Shades-of-Grey method by introducing Minkowski-norm into the Gray-World. van de Weijer et al. [33] proposed the Gray-Edge hypothesis by analyzing the color derivative distribution of images in opposing color spaces. However, these methods do not solve the problem better. We consider that the foggy environment is similar to the underwater environment, our method refers to white balance method that proposed in Ancuti *et al.* [34]

to correcting the color casts caused by different color illumination on the defogged image.

Therefore, in our method, the value of the illumination μ_I is estimated by calculating the average of the scene μ_r and the adjustment of the parameter α.

$$\mu_I = 0.5 + \alpha\mu_r \quad (21)$$

where μ_r is used to estimate the color of the illumination color, and α is employed to adjust μ_r. Although it is simple, this white balance method effectively eliminates the color casts and also restores the white and grays shades of the defogged image.

III. EXPERIMENTAL RESULTS
The proposed method is implemented on a PC-Windows 10 platform with an Intel (R) Core (TM) i9-9900K CPU @ 3.6 GHz processor and 16GB RAM, and running software is MATLAB R2014a. In this paper, natural images in foggy conditions are randomly selected for testing, and the images are derived from NASA's open image, dataset and a previous standard dataset [5], [21], [26], [29]. The analysis of the experiment results mainly includes implementation details and overall performance analysis of this method including qualitative and quantitative comparisons, while outputting a defogged image with a better natural appearance.

A. SELECT THE NUMBER OF GAUSSIAN KERNELS
In section *B*, we explained in detail that the key step of the MSRCR method is the estimation of the illumination component. In order to verify the effect of the enhanced performance of MSRCR with different scales and numbers of Gaussian kernel functions. The foggy image, defogged image, and local amplification effect as shown in Fig. 3. The parameters and results of the MSRCR method are shown in Table 1. In terms of subjective analysis, the MSRCR method not only achieves better defogging, but improves brightness and contrast as shown in the first row of Fig. 3. When $kernel \ge 6$, the MSRCR method has good detail enhancement ability, and it is difficult to see the difference from subjective effect with the increase of Gaussian kernels. In terms of objective analysis, when $kernel \ge 6$, the qualitative metrics of average gradient(*AG*) [35], information entropy(*IE*) [35], and edge preservation index(*EPI*) [36] of the MSRCR method are greatly improved. As the number of kernel increases, the qualitative metrics of MSRCR is rises slowly and tends to be stable, but the running time (*RT*) is also increasing. The effect and running time of MSRCR are considered comprehensively, and $kernel = 6$ is finally determined.

B. MULTI-CHANNEL CONVOLUTION
In this paper, the multi-channel convolution is mainly to extract the precise feature to estimate the illumination component. To evaluate the performance of the multi-channel convolution, the three scales of the MSRCR are $\sigma_1 = 40$, $\sigma_2 = 80$ and $\sigma_3 = 160$, respectively. And the six scales of the MC module are $\sigma_1 = 40$, $\sigma_2 = 80$, $\sigma_3 = 60$, $\sigma_4 = 80$,

TABLE 1. Average gradient, information entropy, edge preservation index, and running time of the MSRCR method when the number of kernels is 3, 6, 9 and 12, respectively.

Kernels	Scales	AG	IE	EPI	RT(s)
3	40 60 160	3.00	7.09	4.00	0.34
6	20 40 60 80 120 160	3.38	7.28	4.50	0.76
9	10 20 40 60 80 100 120 160 180	3.47	7.30	4.61	1.05
12	10 20 30 40 60 80 100 120 130 150 170 200	3.49	7.31	4.63	1.32

FIGURE 3. The first row is the original image, and the defogged images of MSRCR when the number of kernels is 3, 6, 9 and 12, respectively. The second row is the local amplification effect of the red box area in the first column.
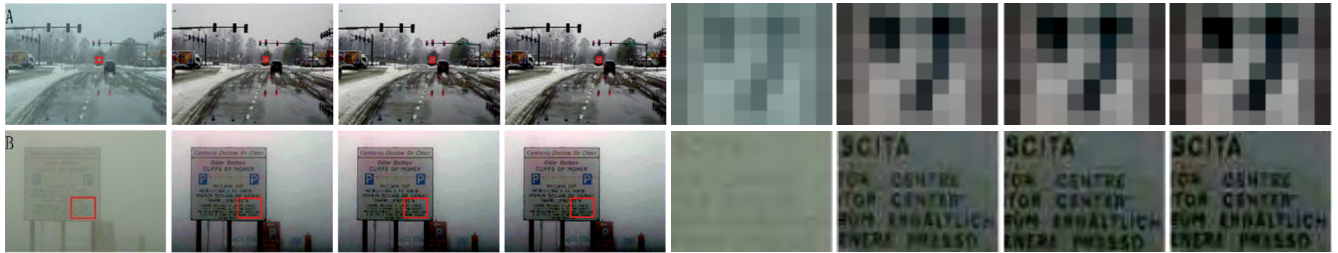

FIGURE 4. From left to right: the original images A and B, and the defogged images are obtained by MSRCR, multi-channel convolution, the local amplification effect of the red box of the original images, the local amplification effect of the red box of the defogged images are obtained by MSRCR, and multi-channel convolution.

$\sigma_5 = 120$ and $\sigma_3 = 160$, respectively. The dense fog images A and B of two different scenes are selected as test sample, as shown in the first column of Fig. 4. For both A and B scenarios, MSRCR and MC module have better defogging effects than the original image in the second and third columns. However, the car, road surface, and trees are clearer in the A scene of the third column, and the reflected lights of the car are bright. The billboard and car are clearer in the B scene of the third column, and the billboard with better color fidelity. In terms of detail enhancement, the road signs and words are clear and the details are prominent in the red area of the A and B scenes of the sixth column. The experimental results show that the MC module effectively enhances the detail and contrast, and improves the overall visual effect of the image.

C. SECONDARY GUIDED FILTER

In this part, in order to verify the performance of the secondary guided filter, the dense fog images A and B of two different scenes are selected as test sample, as shown in the first column of Fig. 5. Here, $r = 32$ and $\varepsilon = 0.01$ of first guided filter operation and secondary guided filter, and the detailed solution in He *et al.* [20]. For both A and B scenarios, MSRCR, MC module, and secondary guided filter have better defogging effects than the original image in the A and B scenes of the second, third, and fourth columns. And, the results of the MSRCR and MC operation have been given in section *B*. In terms of the overall defogging effect, it is difficult to see from the visual effect that the secondary guided filter module is superior to the MC module. However, in terms of detail enhancement, it can clearly see that the road

FIGURE 5. From left to right: the original images A and B, and the defogged images obtained by MSRCR, multi-channel convolution operation, secondary guided filter, the local amplification effect of the red box of the original images, the local amplification effect of the red box of the defogged images are obtained by MSRCR, multi-channel convolution, and secondary guided filter.

FIGURE 6. From left to right: the original images A and B, and the defogged images are obtained by secondary guided filter, white balance operation.

signs and words of the eighth column are significantly better than the sixth and seventh columns in the A and B scenes, and the contrast enhancement of the road signs and words are clearer in the eighth column. The experimental results show that the secondary guided filter effectively enhances the image detail, the noise in the enhanced image is reduced and improves the overall visual effect of the image.

D. WHITE BALANCEING OF THE DEFOGGED IMAGES

In this part, in order to verify the performance of the white balance, the dense fog images A and B of two different scenes are selected as test sample, as shown in the first column of Fig. 6. We have described the effect of Secondary guided filter in detail in Section C, this section mainly introduces the effect of white balance. In the third column of the A scene, we can clearly see that the defogged image processed by white balance is better eliminate red color and improves the visual effect of the defogged image. In the third column of the B scene, we can clearly see that the defogged image has better visual effects and sharpness.
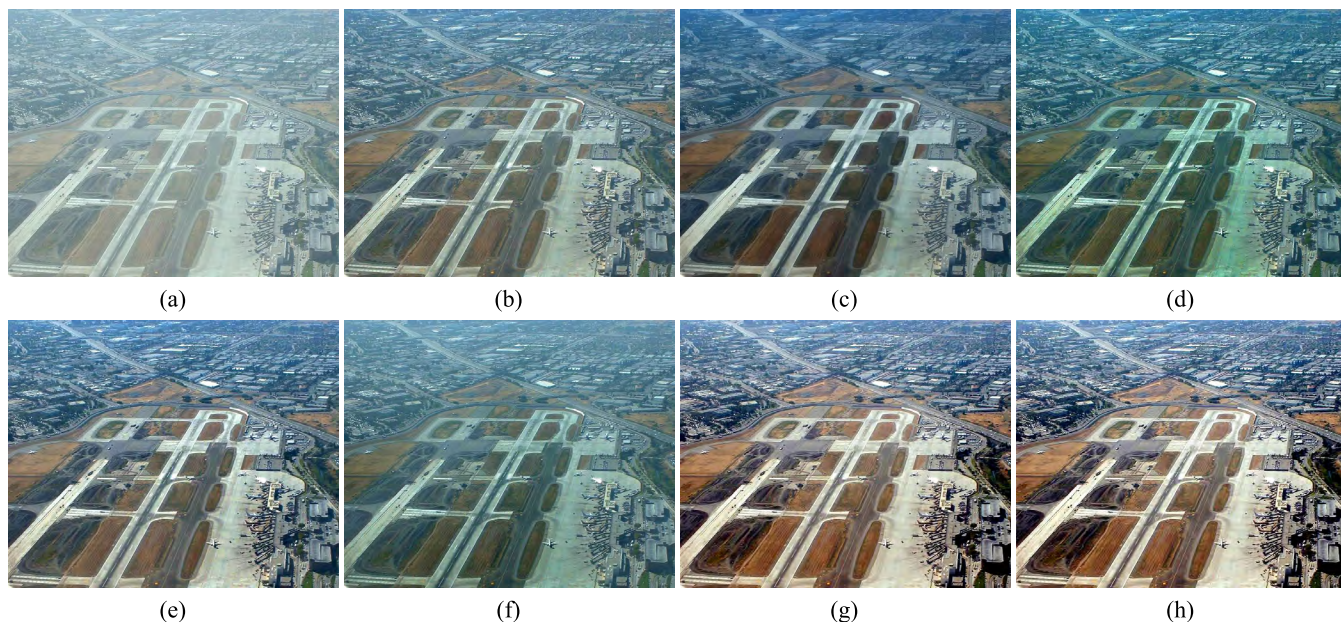
E. QUALITATIVE COMPARISON

We first analyze the qualitative results of the proposed defogging method. The defogged images can be divided into five categories based on different scenarios, including airport, factory, highway, billboard and underwater.

We compare the performance of the proposed method with state-of-the-art methods: Zhu*et al.* [5], Chen*et al.* [15],
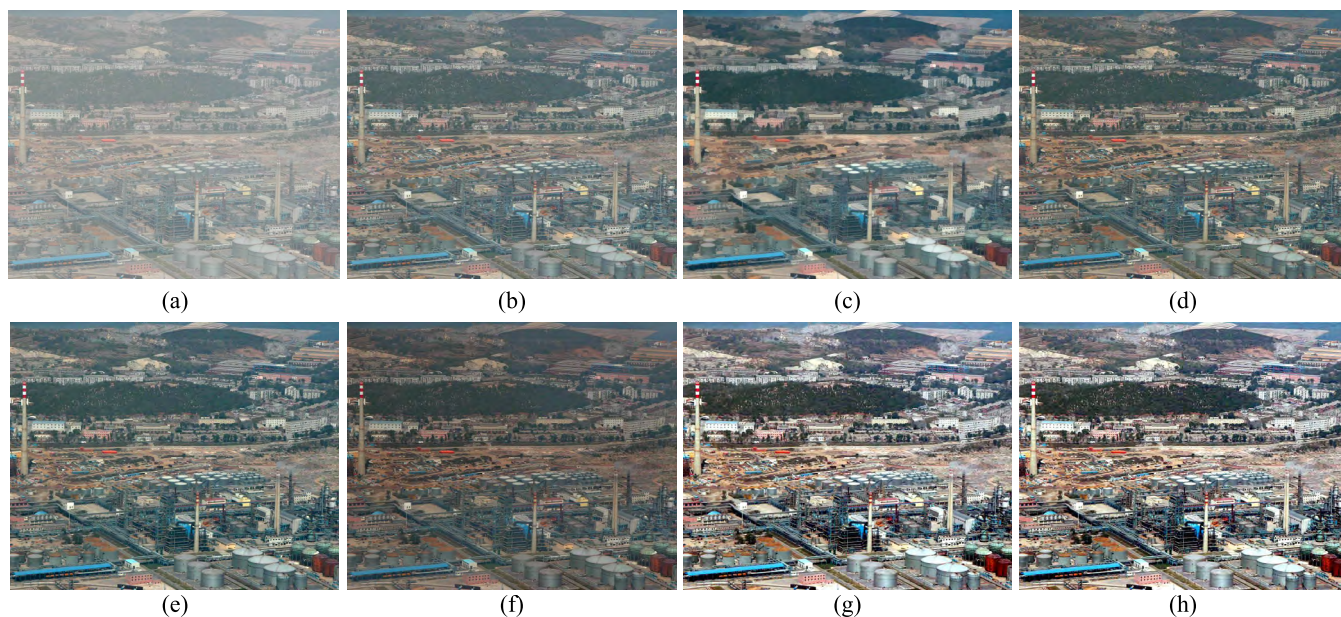
He*et al.* [20], Ren*et al.* [27], Cai*et al.* [29], and Wang*et al.* [26], the results are shown in Fig.7-Fig.10. It can be clearly seen that all of these defogging methods get good defogged results, and these fog-free images can achieve better defogging effects, and the fog-free images achieve contrast enhancement with more detail information. The following is a comparison and analysis of Fig.7-Fig.11, from two aspects of overall vision and local details, respectively.

In term of overall vision, the results of the defogged images are shown in the Fig.7 (a-h). The images defogged by He *et al.* [20] and Cai *et al.* [29] are shown in the Fig.7 (d) and (f). It can be observed that the enhanced images have color distortion and halo artifacts. Fig.7 (b) is defogged image result by Zhu *et al.* [5]. It can be seen that the defogging effect is bad and the defogged image detail information is missing. Fig.7 (c) and (e) are defogged images by Chen *et al.* [15] and Ren *et al.* [27]. It can be seen that the dark channel over-enhancement occurs and the image detail information is missing. Fig.7 (g) and (h) are defogged images by Wang *et al.* [26] and our method. It can be observed that these methods achieved better defogging effect, effectively suppressing halo artifacts and enhancing color, but the Wang *et al.* [26] has a slightly worse defogging effect on the airport's prospect area. Fig.7 (h) show the image defogged by the proposed method, which is clear and removes color distortion phenomenon. In terms of local detail, the road sign is clearer, colorful, and the contrast between the light and dark areas is more obvious by our method. It can be seen that the image defogged by the proposed method shows more detail information compared to Wang *et al.* [26].

In Fig.8, the images defogged by Zhu *et al.* [20], He *et al.* [20], and Cai *et al.* [29] are shown in the Fig.8 (b), (d) and (f). It can be seen that the enhanced images have color distortion and halo artifacts. Fig.8 (c) and (e) are defogged images by Chen *et al.* [15] and Ren *et al.* [27] methods. It can be seen that these methods have better defogging effect, but the fog was not completely removed in the forest area, and the defogging result is bad in the factory area of Fig. 8 (f). Fig.8 (g) and (h) are defogged images by Wang *et al.* [26] and our method. It can be seen that these methods can effectively suppressing halo artifacts and enhancing color. However, our method has better color fidelity, and the defogging effect of our method is superior

FIGURE 7. Qualitative comparison of the proposed method with six other methods. (a) Input hazy image. The defogged images are obtained by (b) Zhu *et al.* [5], (c) Chen *et al.* [15], (d) He *et al.* [20], (e) Ren *et al.* [27], (f) Cai *et al.* [29], (g) Wang *et al.* [26], (h) Proposed method, respectively.
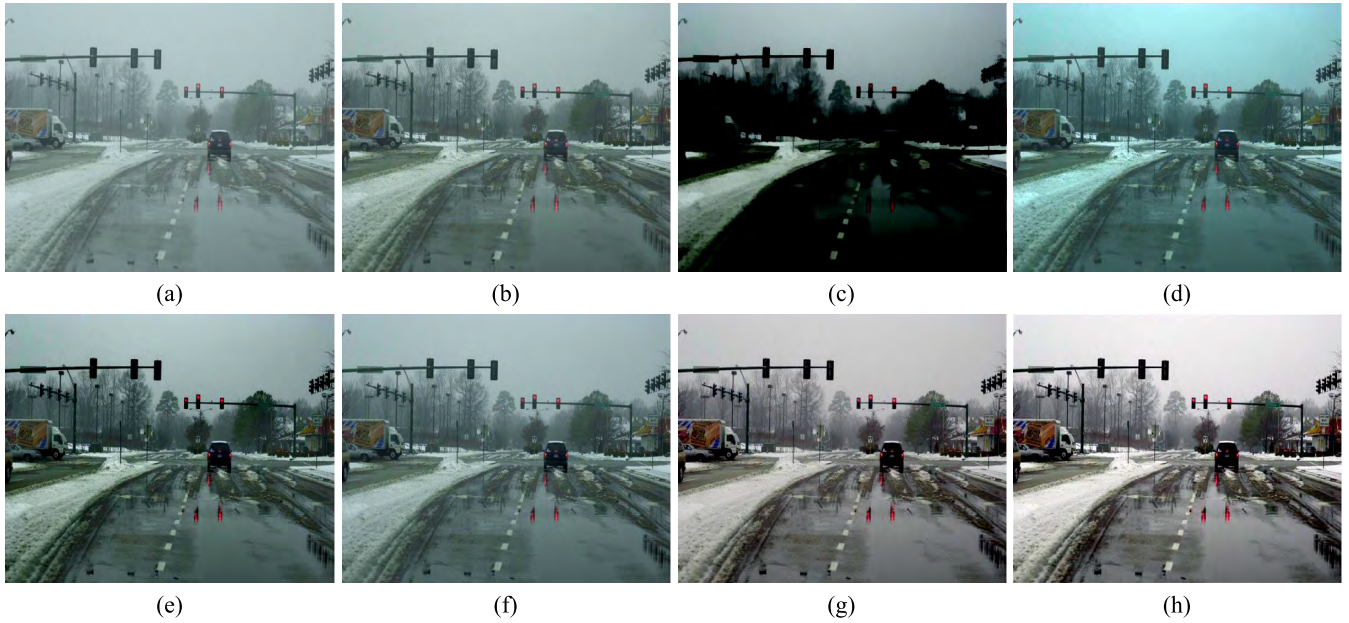

FIGURE 8. Qualitative comparison of the proposed method with six other methods. (a) Input hazy image. The defogged images are obtained by (b) Zhu *et al.* [5], (c) Chen *et al.* [15], (d) He *et al.* [20], (e) Ren *et al.* [27], (f) Cai *et al.* [29], (g) Wang *et al.* [26], (h) Proposed method, respectively.

to Wang *et al* [26] in the forest area. In terms of local detail, the building contour is clear, the forest is colorful, and the contrast between the bright and dark areas in more obvious by our method. It can be seen that the image defogged by our method has more detail information and better visual effects than other methods.

In Fig.9, the image defogged by Chen *et al.* [15] and He *et al.* [20] are shown in the Fig.9 (c) and (d). It can be seen that the dark channel over-enhancement occurs and the

image detail information is missing. Fig.9 (b) and (f) are defogged images by Zhu *et al.* [5] and Cai *et al.* [29]. It can be observed that the defogging effect of these methods is not significant, but Cai *et al.* [29] is better than the Zhu *et al.* [5]. Fig.9 (e), (g) and (h) are defogged images by Ren *et al.* [27], Wang *et al.* [26] and our method. It clearly shows that these methods can effectively remove fog, and the contrast of images Fig. (g) and Fig. (h) is significantly improved compared to Fig. (e). In terms of local detail, the car, road

FIGURE 9. Qualitative comparison of the proposed method with six other methods. (a) Input hazy image. The defogged images are obtained by (b) Zhu *et al.* [5], (c) Chen *et al.* [15], (d) He *et al.* [20], (e) Ren *et al.* [27], (f) Cai *et al.* [29], (g) Wang *et al.* [26], (h) Proposed method, respectively.
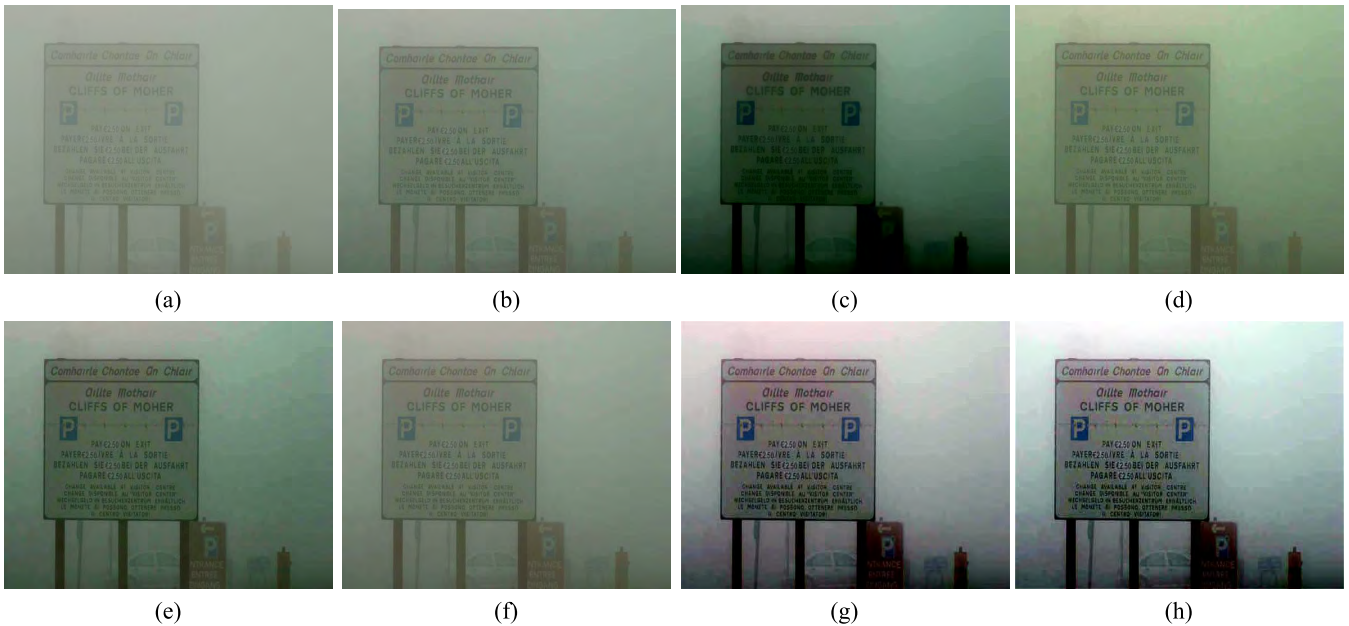
FIGURE 10. Qualitative comparison of the proposed method with six other methods. (a) Input hazy image. The defogged images are obtained by (b) Zhu *et al.* [5], (c) Chen *et al.* [15], (d) He *et al.* [20], (e) Ren *et al.* [27], (f) Cai *et al.* [29], (g) Wang *et al.* [26], (h) Proposed method, respectively.

surface, and trees are clearer by our method, the defogging effect of our method is superior to Wang *et al.* [26] in the prospect area.

In Fig.10, the images defogged by Zhu *et al.* [5], Chen *et al.* [15], He *et al.* [20], and Ren *et al.* [27] are shown in the Fig.9 (b-e). It can be seen that these methods have poor defogging effect, the dark channel of Fig. 10 (c) and Fig. 10 (e) over-enhancement and the image detail information is missing. Fig.10 (g) and (h) are defogged images

by Wang *et al.* [26] and our method. It can be seen that these methods can effectively suppressing halo artifacts and enhancing color, but the red color distortion in Fig. 10 (g). However, our method better suppresses red distortion, the words are clearer by our method, the defogging effect of our method is superior to Wang *et al.* [26] in the billboard area. However, our defogged image also has shortcomings. For example, our method cannot effectively remove fog from the sky, and the words are blurred at the signpost.
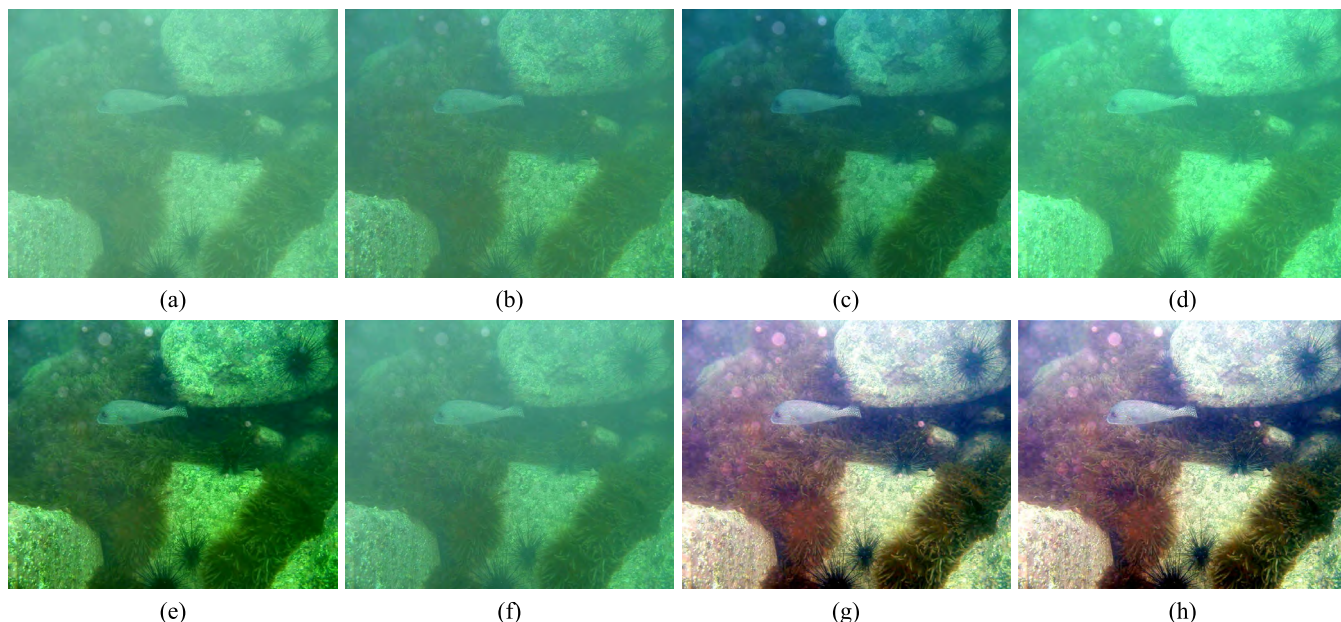
FIGURE 11. Qualitative comparison of the proposed method with six other methods. (a) Input hazy image. The defogged images are obtained by (b) Zhu *et al.* [5], (c) Chen *et al.* [15], (d) He *et al.* [20], (e) Ren *et al.* [27], (f) Cai *et al.* [29], (g) Wang *et al.* [26], (h) Proposed method, respectively.

In Fig.11, the images defogged by Zhu *et al.* [5], He *et al.* [20], and Cai *et al.* [29] are shown in the Fig.11 (b), (d) and (f). It can be seen that these methods have poor defogging effect and the enhanced images have color distortion and halo artifacts. Fig.11 (c) and (e) are defogged images by Chen *et al.* [15] and Ren *et al.* [27] It can be observed that the method has better defogging effect, but it has color distortion and dark channel over-enhancement. Fig.11 (g) and (h) are defogged images by Wang *et al.* [26] and our method, they all have better defogging and visual effects. However, in terms of local detail, the needles of seaweed are clear, with better color fidelity and the contrast between the bright and dark areas is obvious by our method.

Generally, the qualitative comparisons in Fig.7-Fig.11 show that the proposed can effectively remove fog from various types of fog images and obtain more detail information of defogged images. Moreover, our method has also achieved good results for underwater image enhancement.

F. QUANTITATIVE COMPARSION
In this section, we first introduce quantitative metrics and then provide an analysis of the defogging images.

1) QUANTITATIVE METRICS
In order to avoid the bias caused by qualitative analysis, we qualitatively evaluate analyze our method and six other methods. In terms of quantitative evaluation, we compare different methods from three objective metrics: *AG*, *IE*, and *EPI*. *AG* reflects small changes in the details of the image, and the richness of the image information. For an input image $F(i, j)$, *AG* is defined as follows.

$$AG = \frac{1}{(M-1)(N-1)} \sum_{i=1}^{M-1} \sum_{j=1}^{N-1} \sqrt{(\nabla xF(i,j))^2 + (\nabla yF(i,j))^2} \tag{22}$$

where $\nabla xF(i, j)$ and $\nabla yF(i, j)$ are the difference of $F(i, j)$ along the x and y directions, M and N represent the width and height of the input image, respectively. Therefore, the larger the value of the *AG* that more detail information is obtained for the defogged image.

IE reflects the average amount of information, which can quantitatively describe the richness of image color. When an image is not uniform, the probability of any gray-scale value in the image is equal, that is to say, the dynamic range of the image is broader. Therefore, the value of *IE* is the maximum, but in areas where the fog and grayscale are consistent, the value of *IE* is minimal. *IE* is defined as follows.

$$IE = -\sum_{i=0}^{255} p(i) \log_2 p(i) \tag{23}$$

where i is the pixel value, $p(i)$ is the probability of the occurrence of pixels with a pixel value of i in the entire picture. Hence the larger the *IE* value, the richer the color information contained in the image, that is, the better the visual effect of the image.

EPI reflects the change in the gradient at the edge, which can quantitatively describe the sharpness of the edge of the image. *EPI* represents the ability of an enhanced image to maintain the horizontal or vertical edges of the original image. Therefore, the higher the value of *EPI*,

TABLE 2. AG, IE, and EPI of the proposed algorithm with six other algorithms in Fig. 7, 8, 9, 10 and 11.

Method	Fig 7			Fig 8			Fig 9			Fig 10			Fig 11		
	AG	*IE*	*EPI*	*AG*	*IE*	*EPI*	*AG*	*IE*	*EPI*	*AG*	*IE*	*EPI*	*AG*	*IE*	*EPI*
Input	5.49	6.80	1.00	4.33	6.17	1.00	3.28	6.95	1.00	0.75	6.06	1.00	1.69	7.17	1.00
Zhu	8.18	7.24	1.49	6.99	6.79	1.62	4.08	7.17	1.25	1.08	6.44	1.44	2.03	7.07	1.21
Chen	6.09	7.40	1.09	5.57	7.28	1.22	2.47	4.58	0.68	1.03	7.20	1.30	1.79	7.27	1.05
He	9.16	7.45	1.67	8.07	6.97	1.86	4.56	7.54	1.39	1.17	6.72	1.56	2.46	7.56	1.46
Ren	10.76	7.57	1.95	9.37	7.24	2.16	5.39	7.45	1.65	1.79	6.93	2.39	4.23	7.34	2.51
Cai	7.34	7.30	1.34	6.58	6.70	1.52	4.31	7.30	1.31	1.21	6.63	1.61	2.06	7.33	1.22
Wang	12.85	7.71	2.34	15.00	7.60	3.48	5.97	7.27	1.83	3.00	7.09	4.00	5.36	7.39	3.15
Our	**14.98**	**7.80**	**2.76**	**17.26**	**7.80**	**4.08**	**7.62**	**7.53**	**5.15**	**3.85**	**7.53**	**5.15**	**6.28**	**7.81**	**3.76**

the better the edge preservation capacity. *EPI* is defined as follows.

$$EPI = \frac{\sum_{i=1}^{m} |F_1 - F_2|_{filter}}{\sum_{i=1}^{m} |F_1 - F_2|_{original}} \quad (24)$$

where m is the number of pixels of the image, F_1 and F_2 are the grayscale values of the left and right or up and down adjacent cells, respectively.

2) EVALUATION RESULTS AND ANALYSIS

The three quantitative metrics of the defogged images in Table 2. As shown in Table 2, we can clearly see that the three quantitative metrics of Zhu *et al.* [5], He *et al.* [20], Ren *et al.* [27], Cai *et al.* [29], Wang *et al.* [26], and our method are higher than the original images. Although, the three quantitative metrics after Fig. 7 (c), Fig. 8 (c), Fig. 10 (c), and Fig. 11 (c) are enhanced by Chen *et al.* [15] are larger than the original image, the three quantitative metrics are slightly lower than the original image in Fig 9 (c). The results show that Chen *et al.* [15] is not suitable for application to images with rain and fog. In subsection E, it can clearly see that the methods of Zhu *et al.* [5] and Cai *et al.* [29] have poor defogging effect and the defogged images have color distortion and halo artifacts. Since information entropy is determined by the richness of the colors, the information entropy of these two methods is generally lower than other methods. He *et al.* [20] and Ren *et al.* [27] have better defogging effect, but in terms of quantitative metrics is lower than Wang *et al.* [26]. In order to improve the color fidelity of enhanced images, MSRCR introduces color restoration based on MSR. This paper employs quantization operation to restore color and increase overflow judgment. Our proposed method is higher than Wang *et al.* [26] in terms of three objective metrics. In a word, our method has a great improvement on the average gradient, information entropy and sharpness of the original image, and is superior to other methods. These results show that our method has good defogging ability.

G. RUNNING TIME

Running time is an important indicator for the real application of a method. The running time for each method from the beginning to the end of defogging is shown in table 3.

TABLE 3. Time consumption with zhu *et al.* [5], chen *et al.* [15], he *et al.* [20], ren *et al.* [27], cai *et al.* [29], and wang *et al.* [26], and our method.

Image Resolution	Zhu	Chen	He	Ren	Cai	Wang	Our
597 × 368	0.57	66.61	0.47	1.38	1.33	2.35	0.60
585 × 413	0.59	68.54	0.50	1.20	1.37	2.24	0.63
909 × 758	1.58	230.96	1.34	4.22	4.33	6.97	1.97
910 × 689	1.52	214.18	1.23	4.14	4.13	5.81	1.85
918 × 761	1.62	243.74	1.37	4.70	4.57	6.80	2.07

Our method is much faster than Chen *et al.* [15], Ren *et al.* [27], Cai *et al.* [29], and Wang *et al.* [26], and is slightly slower than Zhu *et al.* [5], and He *et al.* [20]. Chen *et al.* [15] introduced Gradient Residual Minimization, which required multiple iterations to obtain the optimal solution, so the running time is longer. Ren *et al.* [27] and Cai *et al.* [29] are deep learning methods. When the model parameters are well trained, their tested time still has no advantage. Wang *et al.* [26] introduced bilateral filtering, which results in a longer running time. With the increase of image resolution, the running time of Chen *et al.* [15], Ren *et al.* [27], Cai *et al.* [29], and Wang *et al.* [26] increases significantly, while the running time of Zhu *et al.* [5], He *et al.* [20], and our method increases slowly. However, the defogging effect of our method is better than Zhu *et al.* [5] and He *et al.* [20].

IV. CONCLUSION

In this paper, a single image defogging method based on multi-channel convolutional MSRCR proposed. Our method mainly consists of four parts: illumination component estimation, guided filter operation, reconstruction of fog-free images, and write balance operation. The proposed method not only ensures the quality of the illumination component, but also the noise in the enhanced image is reduced. In particular, our method improves both qualitative and quantitative performances when compared with the six state-of-the-art methods. However, our method also has two shortcomings. 1) The complexity of the method is increased due to the introduction of multi-channel convolution and guided filter. 2) Since the colors of the fog and the sky are similar, it is difficult to remove fog effectively in the sky area. These issues will be our future work.

REFERENCES

[1] Y. Gao, H.-M. Hu, B. Li, and Q. Guo, "Naturalness preserved nonuniform illumination estimation for image enhancement based on retinex," *IEEE Trans. Multimedia*, vol. 20, no. 2, pp. 335–344, Feb. 2018.

[2] Y. Xu, J. Wen, L. Fei, and Z. Zhang, "Review of video and image defogging algorithms and related studies on image restoration and enhancement," *IEEE Access*, vol. 4, pp. 165–188, Dec. 2016.

[3] Z. Tufail, K. Khurshid, A. Salman, I. F. Nizami, K. Khurshid, and B. Jeon, "Improved dark channel prior for image defogging using RGB and YCbCr color space," *IEEE Access*, vol. 6, pp. 32576–32587, Jun. 2018.

[4] H.-M. Hu, Q. Guo, J. Zheng, H. Wang, and B. Li, "Single image defogging based on illumination decomposition for visual maritime surveillance," *IEEE Trans. Image Process.*, vol. 28, no. 6, pp. 2882–2897, Jun. 2019.

[5] Q. Zhu, J. Mai, and L. Shao, "A fast single image haze removal algorithm using color attenuation prior," *IEEE Trans. Image Process.*, vol. 24, no. 11, pp. 3522–3533, Nov. 2015.

[6] A. Alajarmeh, R. A. Salam, K. Abdulrahim, M. F. Marhusin, A. A. Zaidan, and B. B. Zaidan, "Real-time framework for image dehazing based on linear transmission and constant-time airlight estimation," *Inf. Sci.*, vols. 436–437, no. 8, pp. 108–130, Apr. 2018.

[7] W. Wang, F. Chang, T. Ji, and X. Wu, "A fast single-image dehazing method based on a physical model and gray projection," *IEEE Access*, vol. 6, pp. 5641–5653, Jan. 2018.

[8] S. G. Narasimhan and S. K. Nayar, "Vision and the atmosphere," *Int. J. Comput. Vis.*, vol. 48, no. 3, pp. 233–254, Aug. 2002.

[9] N. Hautière, J.-P. Tarel, and D. Aubert, "Towards fog-free in-vehicle vision systems through contrast restoration," in *Proc. IEEE Conf. Comput. Vis. Pattern Recognit.*, Jun. 2007, pp. 1–8.

[10] J. Kopf, B. Neubert, B. Chen, M. Cohen, D. Cohen-Or, O. Deussen, M. Uyttendaele, and D. Lischinski, "Deep photo: Model-based photograph enhancement and viewing," *ACM Trans. Graph.*, vol. 27, no. 5 pp. 116-1–116-10, Dec. 2008.

[11] Y. Y. Schechner and Y. Averbuch, "Regularized image recovery in scattering media," *IEEE Trans. Pattern Anal. Mach. Intell.*, vol. 29, no. 9, pp. 1655–1660, Sep. 2007.

[12] S. Shwartz, E. Namer, and Y. Y. Schechner, "Blind haze separation," in *Proc. IEEE Comput. Soc. Conf. Comput. Vis. Pattern Recognit.*, vol. 2. Jun. 2006, pp. 1984–1991.

[13] K. He, J. Sun, and X. Tang, "Single image haze removal using dark channel prior," *IEEE Trans. Pattern Anal. Mach. Intell.*, vol. 33, no. 12, pp. 2341–2353, Dec. 2011.

[14] K. Nishino, L. Kratz, and S. Lombardi, "Bayesian defogging," *Int. J. Comput. Vis.*, vol. 98, no. 3, pp. 263–278, Jul. 2012.

[15] C. Chen, M. N. Do, and J. Wang, "Robust image and video dehazing with visual artifact suppression via gradient residual minimization," in *Proc. Eur. Conf. Comput. Vis.*, vol. 9906, 2016, pp. 576–591.

[16] A. L. da Cunha, J. Zhou, and M. N. Do, "The nonsubsampled contourlet transform: Theory, design, and applications," *IEEE Trans. Image Process.*, vol. 15, no. 10, pp. 3089–3101, Oct. 2006.

[17] M. Shakeri, M. H. Dezfoulian, H. Khotanlou, A. H. Barati, and Y. Masoumi, "Image contrast enhancement using fuzzy clustering with adaptive cluster parameter and sub-histogram equalization," *Digit. Signal Process.*, vol. 62, pp. 224–237, Mar. 2017.

[18] L. Xiao, C. Li, Z. Wu, and T. Wang, "An enhancement method for X-ray image via fuzzy noise removal and homomorphic filtering," *Neurocomputing*, vol. 195, pp. 56–64, Jun. 2016.

[19] N. H. Kaplan and I. Erer, "Bilateral filtering-based enhanced pansharpening of multispectral satellite images," *IEEE Geosci. Remote Sens. Lett.*, vol. 11, no. 11, pp. 1941–1945, Nov. 2014.

[20] K. He, J. Sun, and X. Tang, "Guided image filtering," *IEEE Trans. Pattern Anal. Mach. Intell.*, vol. 35, no. 6, pp. 1397–1409, Jun. 2013.

[21] Y. Wang, H. Wang, C. Yin, and M. Dai, "Biologically inspired image enhancement based on Retinex," *Neurocomputing*, vol. 177, no. 177, pp. 373–384, Feb. 2016.

[22] C. Zhou, X. Yang, B. Zhang, K. Lin, D. Xu, Q. Guo, and C. Sun, "An adaptive image enhancement method for a recirculating aquaculture system," *Sci. Rep.*, vol. 7, no. 1, p. 6243, Jul. 2017.

[23] Q. Fu, C. Jung, and K. Xu, "Retinex-based perceptual contrast enhancement in images using luminance adaptation," *IEEE Access*, vol. 6, pp. 61277–61286, Oct. 2018.

[24] J. P. Tare, N. Hautière, A. Cord, D. Gruyer, and H. Halmaoui, "Improved visibility of road scene images under heterogeneous fog," in *Proc. IEEE Intell. Vehicles Symp. (IV)*, Jun. 2010, pp. 478–485.

[25] J. Zhang, Y. Cao, and Z. Wang, "Nighttime haze removal based on a new imaging model," in *Proc. IEEE Int. Conf. Image Process. (ICIP)*, Oct. 2014, pp. 4557–4561.

[26] J. Wang, K. Lu, J. Xue, N. He, and L. Shao, "Single image dehazing based on the physical model and MSRCR algorithm," *IEEE Trans. Circuits Syst. Video Technol.*, vol. 28, no. 9, pp. 2190–2199, Sep. 2018.

[27] W. Ren, S. Liu, H. Zhang, J. Pan, M.-H. Yang, and X. Cao, "Single image dehazing via multi-scale convolutional neural networks," in *Proc. Eur. Conf. Comput. Vis.*, 2016, pp. 154–169.

[28] Y. Song, J. Li, X. Wang, and X. Chen, "Single image dehazing using ranking convolutional neural network," *IEEE Trans. Multimedia*, vol. 20, no. 6, pp. 1548–1560, Jun. 2018.

[29] B. Cai, X. Xu, K. Jia, C. Qing, and D. Tao, "DehazeNet: An end-to-end system for single image haze removal," *IEEE Trans. Image Process.*, vol. 25, no. 11, pp. 5187–5198, Nov. 2016.

[30] H. Y. Zhao, J. Liu, Z.-J. Zhang, H. Liu, and S. H. Zhou, "Linear fusion for target detection in passive multistatic radar," *Signal Process.*, vol. 130, pp. 175–182, Jan. 2017.

[31] Y. Yang, W. Wan, S. Huang, F. Yuan, S. Yang, and Y. Que, "Remote sensing image fusion based on adaptive IHS and multiscale guided filter," *IEEE Access*, vol. 4, pp. 4573–4582, Aug. 2016.

[32] G. D. Finlayson and E. Trezzi, "Shades of gray and colour constancy," in *Proc. 12th Color Imag. Conf. Final Program*, 2004, pp. 37–41.

[33] J. van de Weijer, T. Gevers, and A. Gijsenij, "Edge-based color constancy," *IEEE Trans. Image Process.*, vol. 16, no. 9, pp. 2207–2214, Sep. 2007.

[34] C. O. Ancuti, C. Ancuti, C. De Vleeschouwer, and P. Bekaert, "Color balance and fusion for underwater image enhancement," *IEEE Trans. Image Process.*, vol. 27, no. 1, pp. 379–393, Jan. 2018.

[35] N. He, J.-B. Wang, L.-L. Zhang, and K. Lu, "An improved fractional-order differentiation model for image denoising," *Signal Process.*, vol. 112, pp. 180–188, Sep. 2015.

[36] W. Dan, Z. Li, L. Cao, V. E. Balas, N. Dey, A. S. Ashour, P. McCauley, S.-P. Dimitra, and F. Shi, "Image fusion incorporating parameter estimation optimized Gaussian mixture model and fuzzy weighted evaluation system: A case study in time-series plantar pressure data set," *IEEE Sensors J.*, vol. 17, no. 5, pp. 1407–1420, Mar. 2017.

WEIDONG ZHANG received the B.S. degree in computer science and technology from the Xinke College of Henan Institute of Science and Technology, Xinxiang, China, in 2015, and the M.S. degree in computer science and technology from the Guilin University of Electronic Technology, Guilin, China, in 2018., He is currently pursuing the Ph.D. degree in information and communication engineering with Dalian Maritime University, Dalian, China. He has authored (coauthored) four research papers. His main research interests include image enhancement and defogging, and target recognition.

LILI DONG was born in Qi Tai He City, Hei Long Jiang, China, in 1980. She received the B.S. degree in mechanical design manufacturing and automation, the M.S. degree from the College of Information Science and Technology, Dalian Maritime University (DLMU), and the Ph.D. degree in instrument science and technology from the Harbin Institute of Technology, Harbin, China, in 2002, 2004, and 2008, respectively. From 2005 to 2008, she was a Teaching Assistant with the College of Information Science and Technology, DLMU, Dalian, China. From 2008 to 2012, she was a Lecturer with the College of Information Science and Technology, DLMU. Since 2012, she has been an Assistant Professor with the Mechanical Engineering Department. She has authored 13 articles and three inventions. Her research interests include multispectral target recognition, tunnel lighting, and photoelectric detection.

XIPENG PAN received the B.S. degree in automation and the M.S. degree in pattern recognition and intelligent system from the Guilin University of Electronic Technology, Guilin, China, in 2007 and 2013, respectively. He is currently pursuing the Ph.D. degree in control science and engineering with the Beijing University of Posts and Telecommunications, Beijing, China. He has authored (coauthored) seven research papers. His main research interests include machine learning and digital image processing.

LI QIN received the B.S. degree in electronic information science and technology, and the Ph.D. degree in information and communication engineering from Dalian Maritime University, Dalian, China, in 2013 and 2019, respectively. From 2017 to 2018, she continued her research with the University of Houston, Houston, TX, USA, as a Joint Ph.D. student. Since 2019, she has been a Lecture with the College of Information Science and Engineering, Ningbo University. She has authored (coauthored) eight research papers. Her research interests include photoelectric detection, sensors control, and digital image processing.

WENHAI XU received the B.S. and M.S. degrees in precision instrument and the first Ph.D. degree in imprecision instrument from the Harbin Institute of Technology, Harbin, China, in 1982, 1984, and 1991, respectively, and the second Ph.D. degree in manufacturing machine from the Tokyo Institute of Technology, Tokyo, Japan, in 1993. From 1986 to 1988, he was a Lecturer with the Harbin Institute of Technology and an Assistant Professor, from 1992 to 2001. He was a Professor with the Harbin Institute of Technology for four years, since 2001. He was the Project Director with Cannon Inc., Tokyo, Japan, from 1993 to 2003. He was also a Research Scientist with System Engineers Company Ltd., Yamato City, Japan, from 1995 to 1997. He is currently a Professor of Opt-Electric Information Science and Engineering with Dalian Maritime University, Dalian, China. In the last ten years, he has directed over 30 research projects and applied 10 national patents. He has authored over 80 research papers. His research interests include infrared detection, digital image processing, design of high-resolution optical imaging systems, and opt-electronic information processing.

JINGCHUN ZHOU received the B.S. degree in computer science and technology from Daqing Normal College, Daqing, China, in 2012, and the M.S. degree in software engineer from the Beijing University of Posts and Telecommunications, Beijing, China, in 2016. He is currently pursuing the Ph.D. degree in technology of computer application with Dalian Maritime University, Dalian, China. His current research interests include image enhancement and fusion.

• • •